Applied Physics Letters

# Annealing effects on sulfur vacancies and electronic transport of $MoS_2$ films grown by pulsed-laser deposition

Cite as: Appl. Phys. Lett. **115**, 121901 (2019); https://doi.org/10.1063/1.5116174
Submitted: 22 June 2019 . Accepted: 04 September 2019 . Published Online: 17 September 2019

M. Z. Xie (谢明章 ), J. Y. Zhou, H. Ji (纪桓 ), Y. Ye (叶艳 ), X. Wang (汪翔 ), K. Jiang (姜凯 ), L. Y. Shang (商丽燕 ), Z. G. Hu (胡志高 ), and J. H. Chu (褚君浩 )

Applied Physics Letters ARTICLE scitation.org/journal/apl

# Annealing effects on sulfur vacancies and electronic transport of $MoS_2$ films grown by pulsed-laser deposition

Cite as: Appl. Phys. Lett. **115**, 121901 (2019); doi: 10.1063/1.5116174
Submitted: 22 June 2019 · Accepted: 4 September 2019 ·
Published Online: 17 September 2019



M. Z. Xie (谢明章),[1] J. Y. Zhou,[1] H. Ji (纪桓),[1] Y. Ye (叶艳),[1] X. Wang (汪翔),[1] K. Jiang (姜凯),[1] L. Y. Shang (商丽燕),[1] Z. G. Hu (胡志高),[1,2,3,a)] and J. H. Chu (褚君浩)[1,2,3]

## AFFILIATIONS

[1]Technical Center for Multifunctional Magneto-Optical Spectroscopy (Shanghai), Department of Electronic Engineering, East China Normal University, Shanghai 200241, China
[2]Collaborative Innovation Center of Extreme Optics, Shanxi University, Taiyuan, Shanxi 030006, China
[3]Shanghai Institute of Intelligent Electronics & Systems, Fudan University, Shanghai 200433, China

[a)]Electronic mail: zghu@ee.ecnu.edu.cn

## ABSTRACT

We have synthesized high quality and large area $MoS_2$ films on flexible fluorophlogopite substrates using the pulsed-laser deposition (PLD) technique. Annealing in a sufficient sulfur atmosphere was adopted to eliminate oxide molybdenum and sulfur vacancies introduced during the growth in the vacuum chamber. X-ray photoelectron spectroscopy results demonstrate the advantages benefitted from the annealing process. The S/Mo ratio of the annealed $MoS_2$ film was 1.98:1, which was much closer to the theoretical value. Raman spectroscopy, Photoluminescence spectroscopy, and X-ray diffraction spectroscopy provided direct evidence for the crystallinity improvement. Due to the elimination of molybdenum oxide, the Fermi level was shifted by 0.175 eV, and the conductive type changes from the Ohmic contact to the Schottky contact. The optimized method in this paper makes the PLD-derived $MoS_2$ films promising candidates for microelectronic device application.



In the past ten years, two-dimensional materials, especially graphene, have attracted extensive research due to their unique chemical and physical properties. Due to the lack of an intrinsic energy bandgap required for transistors, graphene is not widely used in device applications.[1–3] In contrast, two-dimensional transition metal dichalcogenide (TMD) materials have a tunable bandgap from direct to indirect by varying the number of layers.[4] Among them, $MoS_2$ has been the most extensively studied object for its fundamental properties[5–8] and potential applications, such as transistors,[4,9,10] solar cells,[11] detectors,[12,13] batteries,[14] supercapacitors,[15] and so on. In previous works, molybdenum disulfide nanosheets were obtained by various methods, including chemical[16] and mechanical exfoliation,[10] chemical vapor deposition (CVD),[17,18] and physical vapor deposition (PVD).[19] The chemical and mechanical exfoliated $MoS_2$ nanosheets have the best performance, but they are not suitable for practical applications because of their uncontrollable thickness, size, and geometry. For CVD, its main disadvantage is the extreme demand for the growth environment, leading to low repeatability.[20] Therefore, finding a way to provide stable output that meets industrial production requirements remains a challenge.

The pulsed-laser deposition (PLD) technique, an alternative way to the CVD method, can just be used for preparing large scale, thickness-controllable two-dimensional films with high yield and low cost. During the preparation process, the target absorbs the energy of the laser, producing a featherlike plasma stoichiometrically proportional to the target, transferring to the surface of the substrate. Hence, $MoS_2$ films of different thicknesses and sizes and grown on different substrates can be produced.[20–25] The growth temperature of $MoS_2$ films by PLD is mostly around 700 °C. It is well known that high temperature facilitates the crystallization of molybdenum disulfide but causes more loss of sulfur components in a sulfur-free and not completely oxygen-free environment.[19,24]

Therefore, it is difficult to prepare a $MoS_2$ film containing no sulfur vacancies and molybdenum oxide using the PLD technique. Serna *et al.* have tried to compensate the sulfur loss during the film deposition process by incorporating excess sulfur into the targets,

which made it difficult to fabricate targets.[21] Another method, postannealing in a sulfur atmosphere, works in other forms of growth processes, believed to be a valuable way to improve the $MoS_2$ films grown by PLD.[18,25]

In this letter, we prepared several $MoS_2$ films with different thicknesses grown on fluorophlogopite mica ($KMg_3AlSi_3O_{10}F_2$) as a van der Waals (vdW) epitaxy substrate. To obtain an atomically smooth surface, surface layers were removed before the mica substrates were put into use. A commercial target was utilized with a S/Mo ratio of 2:1. A pulsed KrF excimer laser was used with an energy fluence of 4 J/cm$^2$ to ablate the $MoS_2$ target with a repetition rate of 5 Hz. The vacuum chamber has a base pressure higher than $1 \times 10^{-5}$ Pa. The substrates were kept at a temperature of 700 °C and 55 mm away from the target. Flowing Argon with a pressure of 1.5 Pa was used as process gas to attenuate the energy of ions bombarded from the target. During the deposition process, the holder of substrates was rotated to improve the flatness of the film. For comparison, the as-grown films were annealed in a tube furnace in a sulfur atmosphere. During the annealing process, the samples were heated at different temperatures, while the excess sulfur was heated to 200 °C with an argon flow rate of 100 sccm (standard cubic centimeter per minute).

Figure 1(a) shows the atomic force microscopy (AFM) image and the optical picture for the as-grown film deposited on a centimeter-scale fluorophlogopite substrate. The atomic force microscopy (AFM) image shows the height profile of the as-grown $MoS_2$ film for 100 s, which has a thickness of ~3.3 nm with few layers. The two sides of the step in Fig. 1(a) were analyzed by Raman spectroscopy using a 532 nm laser [Fig. 1(b)]. It is well known that the Raman phonon modes of molybdenum disulfide are related to the number of layers. The frequency differences of the two Raman peaks of the $MoS_2$ film is about 24.5 cm$^{-1}$ corresponding to about 5 layers.[7] So each layer

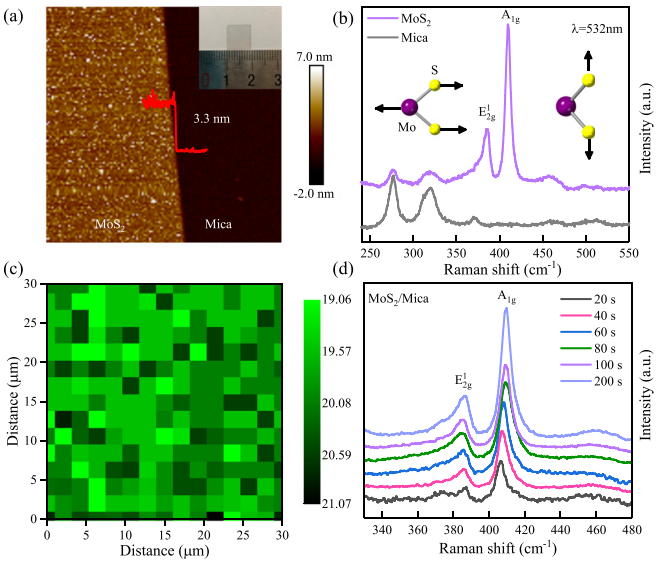


**FIG. 1.** (a) Optical and AFM images of a $MoS_2$ film on a fluorophlogopite mica substrate deposited for 100 s. (b) Raman spectra on both sides of the step (a). (c) Raman mapping of the frequency differences between $E^1_{2g}$ and $A_{1g}$ peaks for a monolayer $MoS_2$ film. (d) Raman spectra of $MoS_2$ films deposited for different times.

of $MoS_2$ deposited by PLD corresponds to about 20 s under the same process conditions. Figure 1(c) shows the Raman mapping of the frequency differences between $E^1_{2g}$ and $A_{1g}$ peaks for a $MoS_2$ film deposited for 20 s. Most of the test points in the figure have a smaller frequency difference than 20 cm$^{-1}$, indicating good flatness with the monolayer. Therefore, $MoS_2$ films of different deposition times corresponding to different layers were prepared [Fig. 1(d)]. As the film thickness increases to 5 layers, the characteristic Raman modes of the in-plane vibration $E^1_{2g}$ and out-of-plane vibration $A_{1g}$ become redshifted and blue-shifted, respectively, which indicates the 2H-$MoS_2$ phase.[7,21] The Raman mappings of the frequency differences between $E^1_{2g}$ and $A_{1g}$ peaks for the 2–5 L $MoS_2$ films have also been studied. The average frequency differences of the 1–5 L $MoS_2$ films are 19.9, 21.4, 22.7, 23.3, and 24.2 cm$^{-1}$, respectively. Simultaneously, the standard deviations of each number of layers are 0.44, 0.45, 0.19, 0.29, and 0.43 cm$^{-1}$, respectively. From the degree of dispersion of the data, we can see that each number of PLD-derived $MoS_2$ layers has good flatness, especially for the 3 L film, which has the best flatness.

As we know, it is difficult to obtain stoichiometry $MoS_2$ films prepared by the PLD method directly. In this letter, annealing in a sulfur atmosphere is employed to improve the quality of $MoS_2$ films. Figure 2(a) shows the schematic diagram of the annealing process. After annealing, X-ray photoelectron spectroscopy (XPS) was used to analyze the valence and composition of both the as-grown and annealed $MoS_2$ films deposited for 100 s [Fig. 2(b)]. The spectra were referenced to C 1s emission at 284.6 eV. It can be seen from the XPS images that the intensity of the hexavalent molybdenum peak of the $MoS_2$ film annealed with 500 °C as the optimum annealing temperature is the weakest. Detailed information can be found from the deconvolutions of XPS spectra. In order to ensure that the fitting results make physical sense, the binding energy difference $\Delta E_B$ of Mo $3d_{5/2}$ and Mo $3d_{3/2}$ was constrained as $3.1 \pm 0.1$ eV, and the area of the former was limited to 3/2 times that of the latter. For sulfur, the binding energy difference $\Delta E_B$ of S $2p_{3/2}$ and S $2p_{1/2}$ was constrained as $1.2 \pm 0.1$ eV, and the area of the former was limited to 2 times that of the latter.[9,19]

As shown in Fig. 2(c), the deconvolution of Mo 3d spectra consists of peaks at 235.9 eV, 232.8 eV, 232.7 eV, 229.6 eV, 228.3 eV, and 226.8 eV. The doublet peaks at 235.9 eV and 232.8 eV are attributed to the $Mo^{6+}$ state of $MoO_3$. The doublet peaks at 232.7 eV and 229.6 eV are attributed to the $Mo^{4+}$ state of 2H-$MoS_2$. The peaks at 226.8 and 228.3 eV belong to the S 2s core level corresponding to the $S^{2-}$ state of $MoS_2$ and other S species such as oxysulfide compounds, $MoS_x$ (with $x \neq 2$) phase, respectively. Comparing the two pictures in Fig. 2(c), it can be found that the peaks of hexavalent molybdenum are significantly reduced after annealing. It is most likely because the imperfect film surface may react with ingredients in the air when exposed to the atmosphere. There were residual little hexavalent molybdenum and abnormal S states in the films after annealing. Figure 2(d) shows that the deconvolution of S 2p XPS peaks includes doublet peaks at 163.6 eV and 162.4 eV corresponding to the S $2p_{1/2}$ and S $2p_{3/2}$ orbitals, respectively. Additional redshift peaks obtained in Fig. 2(d) also suggest the presence of other $S^{2-}$ states in the film, which is weakened after annealing. Such results are consistent with the XPS spectral results of molybdenum.[19,21] For the sulfur to molybdenum ratio, the calculated values of the S/Mo ratio are 1.73 of the as-grown sample and 1.98 of the annealed sample. Simultaneously, the proportion of $Mo^{6+}$ decreased from 5% to 2%. All the results suggest that annealing

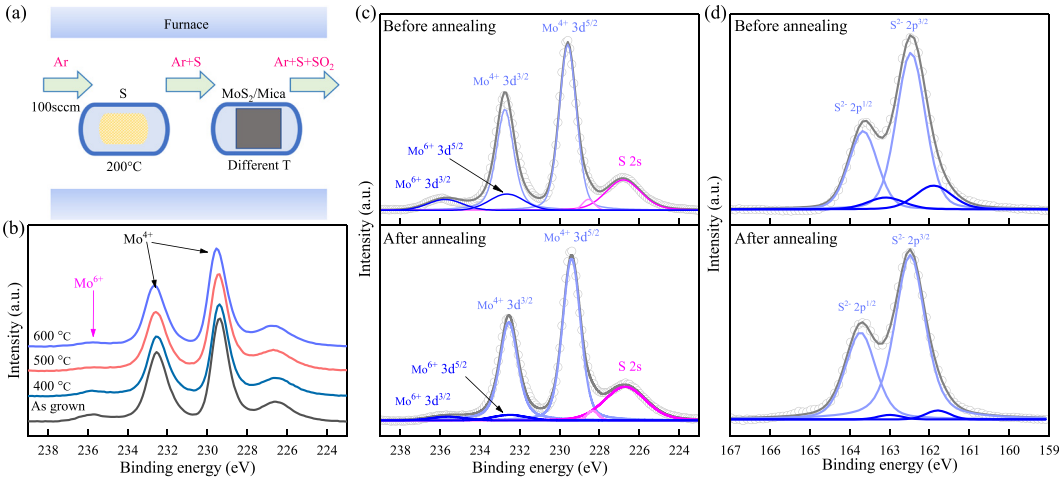


**FIG. 2.** (a) Schematic diagram of the annealing process for $MoS_2$ films at different temperatures. (b) XPS spectra of Mo 3d core level peaks for $MoS_2$ films as-grown and annealed at different temperature. The peak of hexavalent molybdenum at 500 °C is the weakest. (c) The deconvolution of Mo 3d, S 2s, and (d) S 2p core level peaks for $MoS_2$ films before and after annealing at 500 °C. The experimental data are represented by circles, and fitted results are represented by the gray lines.

in a sulfur atmosphere can repair the sulfur vacancies and revulcanized molybdenum oxide at the same time.

The crystallinity of the $MoS_2$ films is also changed after annealing. Figures 3(a) and 3(b) show the scanning electron microscopy (SEM) images of one $MoS_2$ film before and after annealing. The surface still maintains good flatness after annealing. Figures 3(c) and 3(d) show the deconvolution of Raman spectra before and after annealing. For the as-grown one, the full widths at half maximum (FWHM) of modes $E^1_{2g}$ and $A_{1g}$ are 4.05 $cm^{-1}$ and 6.47 $cm^{-1}$, respectively, but decreased to 2.62 $cm^{-1}$ and 4.54 $cm^{-1}$ after annealing, slightly larger than the value from mechanically exfoliated flakes previously reported by Lee *et al.*[7] As the layer number increases, the FWHM values of modes $E^1_{2g}$ and $A_{1g}$ increase as a whole, indicating a deteriorating tendency for the crystallinity, which may be related to the accumulation of the defect during growth. Photoluminescence (PL) spectra in Fig. 3(e) provide a strong evidence of improved crystallinity. Before annealing, no excitonic peaks can be observed on the as-grown $MoS_2$ films except for one from the substrate. However, after annealing, one obvious peak appears around 660 nm (1.88 eV) for the monolayer $MoS_2$. When added to two and three layers, there is another weak peak around 615 nm. Unlike common sense, no significant shifts are observed in the peak position for the bilayer and trilayer sample. At the same time, the PL spectra of bilayer and trilayer $MoS_2$ films have enhanced excitation peaks than the monolayer with the optical band from indirect to direct. These phenomena may be related to the good crystallinity of the bilayer and trilayer $MoS_2$ films and the coexistence with monolayer $MoS_2$ in them using the PLD method, which has been observed from the images of Raman mapping. The X-ray diffraction (XRD) analysis is an evidence of improved crystallinity as well. As shown in Fig. 3(f), the diffraction peak intensity of the $MoS_2$ film obviously increased after annealing, as compared to the as-grown one. The diffraction peak of $MoO_3$ in (020) crystal orientation (JCPDS No. 35-0609, $2\theta = 12.85°$) is near the left side of hexagonal molybdenum sulfide in (002) crystal orientation (JCPDS No. 37-1492, $2\theta = 14.45°$).[26] As we can see, the diffraction peak of the as-grown sample is at

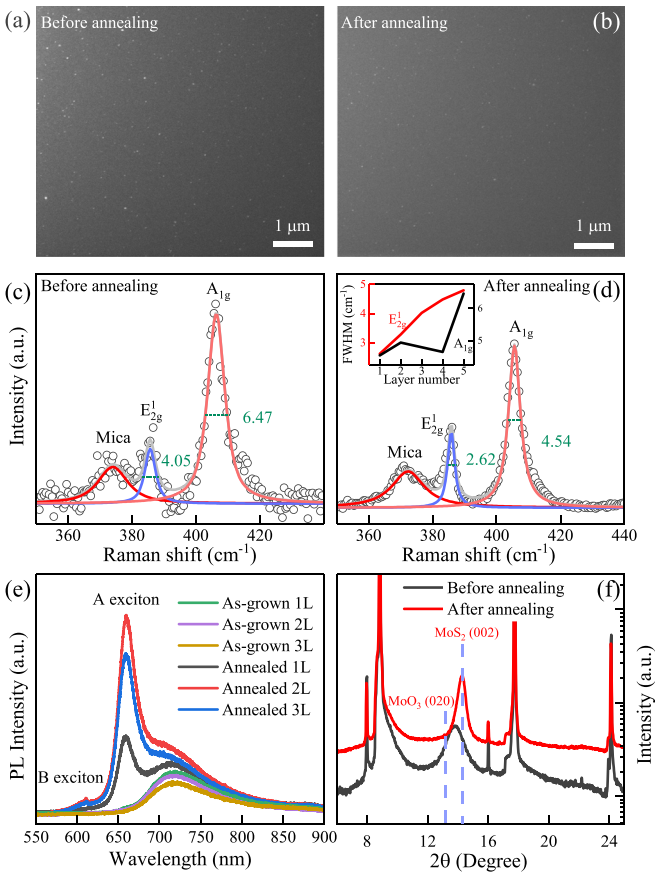


**FIG. 3.** (a) The SEM images of as-grown and (b) annealed $MoS_2$ films at 500 °C. (c) and (d) The Raman, (e) PL, and (f) XRD spectra of the as-grown sample and the sample at 500 °C. The smaller the FWHM, the better the crystallinity.

$2\theta = 13.80°$, between the diffraction peaks of $MoO_3$ in the (020) plane and $MoS_2$ in the (002) plane, indicating the coexistence of $MoO_3$ and $MoS_2$. However, the peak position shifted to the standard peak of the hexagonal $MoS_2$, which indicates that the composition of molybdenum oxide is substantially eliminated after annealing. Meanwhile, the FWHM of the XRD diffraction peak of the annealed sample is also much smaller than the as-grown one. According to the Debye-Scherrer formula, the grain size increased after annealing. In summary, all the SEM images and Raman, PL, and XRD spectra indicate that the annealed $MoS_2$ films have improved crystallinity.

Electrical properties are important for $MoS_2$ films as a semiconductor material. As shown in Figures 4(a) and 4(d) and Figures 4(b) and 4(e), the topography and surface potentials around the Au-$MoS_2$ junctions were studied using AFM and a Kelvin probe force microscope (KPFM). As shown in Figures 4(c) and 4(f), the surface potential differences between monolayer $MoS_2$ and gold are determined to be 65 mV and 240 mV before and after the annealing, respectively. Both the values are smaller than the theoretical difference between monolayer $MoS_2$ ($\Phi_{MoS_2} \approx 4.36$ eV) and gold ($\Phi_{Au} \approx 5.1$ eV),[9] probably because of the large surface states formed by the imperfect surface and the effect of $MoO_3$ existing in the $MoS_2$ film on the work function. Using the surface potential of gold as the reference value, the Fermi level shift is obtained about 0.175 eV, indicating that the calculated work function of $MoS_2$ reduced by 0.175 eV after annealing. Simultaneously, the as-grown $MoS_2$ film forms an Ohmic contact with gold, unlike the annealed $MoS_2$ film, which can be seen from the inset in Figs. 4(c) and 4(d). As mentioned above, the as-grown $MoS_2$ film obtained using the PLD method inevitably contains molybdenum oxide with a work function as high as 6.9 eV and a lot of surface states, which could explain the Ohmic contact between the gold and $MoS_2$ films before annealing and the decrease in the work function of $MoS_2$ films with an approximate Schottky contact after annealing.[27–29] Such results indirectly demonstrate the effect of annealing on the crystallinity of $MoS_2$, consistent with the results of Raman, PL, and XRD spectra.

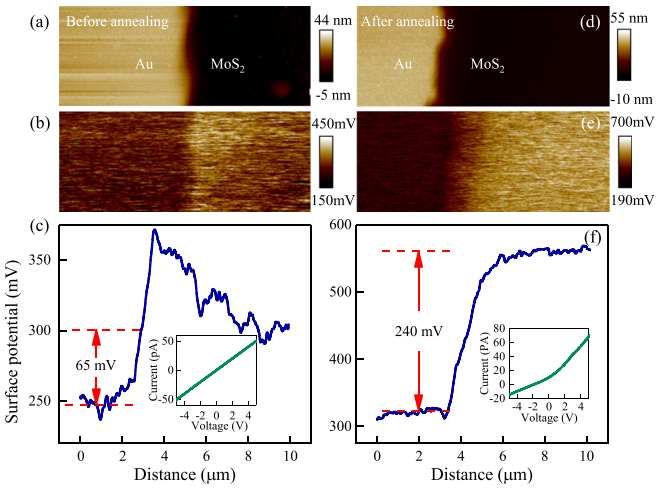


**FIG. 4.** (a) and (d) AFM and (b) and (e) surface potential images for $MoS_2$ films with gold contacts. (c) The surface potential of the profile and I-V characteristic curves for $MoS_2$ films before and (f) after annealing.

In conclusion, we have realized large area and thickness-controllable growth of $MoS_2$ films on the fluorophlogopite substrates using the PLD technique. Furthermore, we managed to reduce molybdenum oxide and sulfur vacancies using annealing under a sulfur atmosphere. After annealing, the S/Mo ratio approached stoichiometry and the crystallinity was improved significantly. PL and XRD spectra provide convincing evidence. Simultaneously, the Fermi level dropped by 0.175 eV and the $MoS_2$ film forms an approximate Schottky contact after annealing, also verifying the advantages of the annealing. These findings provide optimized $MoS_2$ films prepared by PLD leading to further applications.

This work was financially supported by the National Key R&D Program of China (Grant Nos. 2017YFA0303403 and 2018YFB0406500), the Natural Science Foundation of China (Grant Nos. 61674057 and 91833303), Projects of Science and Technology Commission of Shanghai Municipality (Grant Nos. 18JC1412400, 18YF1407200, and 18YF1407000), the Program for Professor of Special Appointment (Eastern Scholar) at Shanghai Institutions of Higher Learning, and the Fundamental Research Funds for the Central Universities.

## REFERENCES

[1]K. S. Novoselov, A. K. Geim, S. V. Morozov, D. Jiang, Y. Zhang, S. V. Dubonos, I. V. Grigorieva, and A. A. Firsov, Science **306**, 666 (2004).
[2]K. Novoselov, A. Geim, S. Morozov, D. Jiang, M. Katsnelson, I. Grigorieva, S. Dubonos, and A. Firsov, Nature **438**, 197 (2005).
[3]G. R. Bhimanapati, Z. Lin, V. Meunier, Y. Jung, J. Cha, S. Das, D. Xiao, Y. Son, M. S. Strano, V. R. Cooper, L. Liang, S. G. Louie, E. Ringe, W. Zhou, S. S. Kim, R. R. Naik, B. G. Sumpter, H. Terrones, F. Xia, and Y. Wang, ACS Nano **9**, 11509 (2015).
[4]B. Radisavljevic, A. Radenovic, J. Brivio, V. Giacometti, and A. Kis, Nat. Nanotechnol. **6**, 147 (2011).
[5]W. Jie, Z. Yang, F. Zhang, G. Bai, C. W. Leung, and J. Hao, ACS Nano **11**, 6950 (2017).
[6]Z. Chi, X. Chen, F. Yen, F. Peng, Y. Zhou, J. Zhu, Y. Zhang, X. Liu, C. Lin, S. Chu, Y. Li, J. Zhao, T. Kagayama, Y. Ma, and Z. Yang, Phys. Rev. Lett. **120**, 037002 (2018).
[7]C. Lee, H. Yan, L. E. Brus, T. F. Heinz, J. Hone, and S. Ryu, ACS Nano **4**, 2695 (2010).
[8]Y. Li, C. Xu, and L. Zhen, Appl. Phys. Lett. **102**, 143110 (2013).
[9]D. J. Late, P. A. Shaikh, R. Khare, R. V. Kashid, M. Chaudhary, M. A. More, and S. B. Ogale, ACS Appl. Mater. Interfaces **6**, 15881 (2014).
[10]Y. Liu, J. Guo, A. Yu, Y. Zhang, J. Kou, K. Zhang, R. Wen, Y. Zhang, J. Zhai, and Z. L. Wang, Adv. Mater. **30**, 1704524 (2018).
[11]A. Arulraja, M. Rameshb, B. Subramanianb, and G. Senguttuvan, Sol. Energy **174**, 286 (2018).
[12]D. Burman, R. Ghosh, S. Santra, S. K. Ray, and P. K. Guha, Nanotechnology **28**, 435502 (2017).
[13]L. Wang, J. Jie, Z. Shao, Q. Zhang, X. Zhang, Y. Wang, Z. Sun, and S. Lee, Adv. Funct. Mater. **25**, 2910 (2015).
[14]M. B. Sreedhara, S. Gope, B. Vishal, R. Datta, A. J. Bhattacharyy, and C. N. R. Rao, J. Mater. Chem. A **6**, 2302 (2018).
[15]P. Sun, R. Wang, Q. Wang, H. Wang, and X. Wang, Appl. Surf. Sci. **475**, 793 (2019).
[16]G. Eda, H. Yamaguch, D. Voiry, T. Fujita, M. Chen, and M. Chhowalla, Nano Lett. **11**, 5111 (2011).
[17]W. Zhang, J. Huang, C. Chen, Y. Chang, Y. Cheng, and L. Li, Adv. Mater. **25**, 3456 (2013).
[18]L. K. Tan, B. Liu, J. H. Teng, S. Guo, H. Y. Low, and K. P. Loh, Nanoscale **6**, 10584 (2014).
[19]J. Liu, A. Goswami, K. Jiang, F. Khan, S. Kim, R. McGee, Z. Li, Z. Hu, J. Lee, and T. Thundat, Nat. Nanotechnol. **13**, 112 (2018).

[20]Z. Yang and J. Hao, J. Mater. Chem. C **4**, 8859 (2016).
[21]M. I. Serna, S. H. Yoo, S. Moreno, Y. Xi, J. P. Oviedo, H. Choi, H. N. Alshareef, M. J. Kim, M. Minary-Jolandan, and M. A. Quevedo-Lopez, ACS Nano **10**, 6504 (2016).
[22]Y. Xie, B. Zhang, S. Wang, D. Wang, A. Wang, Z. Wang, H. Yu, H. Zhang, Y. Chen, M. Zhao, B. Huang, L. Mei, and J. Wang, Adv. Mater. **29**, 1605972 (2017).
[23]Y. Shen, P. Miao, C. Hu, J. Wu, M. Gao, and P. Xu, ChemcatChem. **10**, 3520 (2018).
[24]A. Goswami, P. Dhandaria1, S. Pal, R. McGee, F. Khan, Z. Antić, R. Gaikwad, K. Prashanthi, and T. Thundat, Nano Res. **10**, 3571 (2017).
[25]A. Barvat, N. Prakash, B. Satpati, S. Singha, G. Kumar, D. Singh, A. Dogra, S. Khanna, A. Singha, and P. Pal, J. Appl. Phys. **122**, 015304 (2017).
[26]D. Wang, J. Li, Y. Zhou, D. Xu, X. Xiong, R. Peng, and M. Wang, Appl. Phys. Lett. **108**, 053107 (2016).
[27]D. Liu, Y. Guo, L. Fang, and J. Robertson, Appl. Phys. Lett. **103**, 183113 (2013).
[28]M. Greiner, L. Chai, M. Helander, W. Tang, and Z. Lu, Adv. Funct. Mater. **23**, 215 (2013).
[29]L. Jiao, W. Jie, Z. Yang, Y. Wang, Z. Chen, X. Zhang, W. Tang, Z. Wu, and J. Hao, J. Mater. Chem. C **7**, 2522 (2019).